Congenital Anomalies
THE JAPANESE TERATOLOGY SOCIETY
doi:10.1111/j.1741-4520.2010.00282.x
Congenital Anomalies 2010; **50**, 197–199

CASE REPORT

Severe Peters Plus syndrome-like phenotype with anterior eye staphyloma and hypoplastic left heart syndrome: Proposal of a new syndrome

Reiko Shimizu[1], Ryota Saito[2], Kenji Hoshino[2], Kiyoshi Ogawa[2], Takashi Negishi[3], Jiro Nishimura[4], Norimasa Mitsui[5], Makiko Osawa[1], and Hirofumi Ohashi[5]

[1]Department of Pediatrics, School of Medicine, Tokyo Women's Medical University, Tokyo, and Divisions of [2]Cardiology, [3]Ophthalmology, [4]Plastic Surgery, and [5]Medical Genetics, Saitama Children's Medical Center, Saitama, Japan

ABSTRACT **Peters Plus syndrome is a very rare autosomal recessive condition characterized by ocular defects (typically Peters anomaly) and other systemic major/minor anomalies. Mutations in the *B3GALTL* gene encoding β 1,3-glucosyltransferase have been found in virtually all patients with typical Peters Plus syndrome. We report on a female patient with unusually severe manifestations of Peters Plus syndrome, including anterior eye staphyloma, cleft lip and palate, and hypoplastic left heart syndrome (HLHS). Analysis of the *B3GALTL* gene revealed no mutation in the patient. To our knowledge, HLHS has not previously been reported in Peters Plus syndrome so far, and anterior staphyloma, a most severe defect of the anterior eye chamber, is also apparently rare in the syndrome. Our patient might represent a new syndrome of severe Peters Plus syndrome-like phenotype with anterior eye staphyloma and HLHS.**

Key Words: anterior staphyloma, hypoplastic left heart syndrome, Peters anomaly, Peters Plus syndrome

INTRODUCTION

Peters Plus syndrome (MIM 261540) is a rare autosomal recessive disease characterized by ocular anterior chamber defects (typically Peters anomaly), distinctive facies (prominent forehead, hypertelorism, narrow palpebral fissure, long philtrum, cupid bow upper lip and malformed ears), cleft lip and palate, short hands and feet, and growth and developmental delay. Since the first detailed delineation of the syndrome by van Schooneveld *et al.* (1984), who coined the term 'Peters Plus syndrome', on the basis of 11 patients with anterior chamber cleavage defect and other multiple congenital anomalies, more than 60 patients have been reported to date. Recently, the syndrome was found to be caused by mutations in β1,3 glucosyltransferase like gene (*B3GALTL*) which codes for glucosyltransferase, β3Glc-T, suggesting that the syndrome is a glycosylation disorder (Lesnik Oberstein *et al.* 2006; Reis *et al.* 2008).

Congenital heart defects are occasionally found in the syndrome, at a frequency of around 30%, including atrial septal defect, ventricular septal defect, subvalvular aortic stenosis, pulmonary stenosis, and bicuspid pulmonary valve (Maillette de Buy Wenniger-Prick and Hennekam 2002). To our knowledge, however, hypoplastic left heart syndrome (HLHS) has not been previously described in the syndrome. Here we report a Japanese girl with Peters Plus syndrome-like phenotype and HLH. In addition, the patient had anterior eye staphyloma, a most severe developmental defect of the anterior eye chamber.

Correspondence: Reiko Shimizu, MD, PhD, Department of Pediatrics, School of Medicine, Tokyo Women's Medical University, 8-1 Kawada-cho, Shinjuku-ku, Tokyo 160-0022, Japan. Email: rmuto@ped.twmu.ac.jp
Received January 5, 2010; revised and accepted May 6, 2010.

CLINICAL DETAILS

The patient, a female, was born by normal delivery after an uneventful 37-week pregnancy to a 32-year-old, gravid 3, para 1, abortus 1 mother and a 34-year-old father, both Japanese, healthy and unrelated. No polyhydroamnios was noted in the pregnancy. The patient had a healthy elder brother. Her birth weight was 2390 g (−1.7 SD), length 46.2 cm (−1.4 SD) and occipitofrontal circumference (OFC) 32.0 cm (± 0 SD). Soon after birth, it was noticed that she had bilateral cleft lip and palate, and corneal opacity of both eyes. Other features also noted were a round face, a narrow forehead, hypertelorism, micrognathia, malformed ears, right preauricular pit, short broad hands, short fifth fingers with single flexion crease and hyperextensible finger joints (Fig. 1). No apparent rhizomelic limb shortening was noticed. Ophthalmological examination revealed anterior staphyloma of both eyes, lacking apparent anterior chamber structures (Fig. 2). On B-mode ultrasonography, both eyeballs were found to be small (around 12 mm), while optic nerves were normally observed.

The day after birth, the patient showed tachypnea and cyanosis and was admitted to our hospital on the suspicion of congenital heart defect. On admission, her weight was 2466 g (76 g gain in one day after birth) in spite of poor intake, heart rate 160/min, respiratory rate 70/min, and SpO_2 95% in room air. Cardiothoracic ratio (CTR) was 56% on a chest X-ray. Echocardiography revealed HLHS with aortic and mitral atresia and a large patent ductus arteriosus (Fig. 3). Despite intensive care, including prostaglandin E1 infusion, she died of ductal shock at the age of 15 days. A post-mortem autopsy was not granted and histopathological investigation for eyes was not performed. Although we could not perform thorough imaging studies, such as total skeletal survey and abdominal echography, no vertebral and urogenital anomalies were noted in the patient.

Chromosome analysis on lymphocytes revealed a normal 46, XX karyotype. Polymerase chain reaction (PCR) and direct sequencing analysis of the *B3GALTL* gene using genomic DNA obtained from residual peripheral blood used for chromosome analysis revealed no

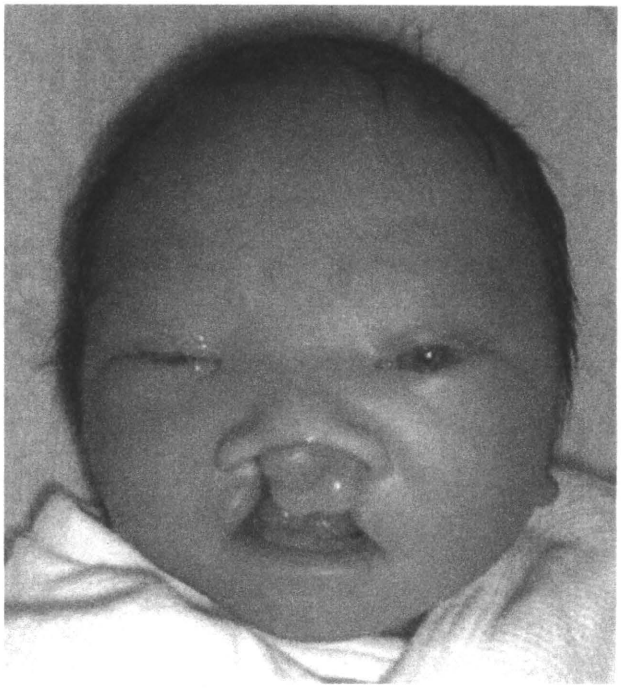

Fig. 1 Craniofacial view of the patient. (Permission for the presentation of this picture was obtained from the patient's parents.)

mutation in any exons or splice sites of the gene in the patient. Unfortunately, we could not perform further studies due to lack of specimen, such as array comparative genomic hybridization and multiplex ligation-dependent probe amplification to evaluate subtle genomic imbalance.

DISCUSSION

HLHS is a serious congenital heart defect characterized by severe underdevelopment of the left side heart structure with a prevalence of 1.4–3.8% among all congenital heart defects. The cause is unknown but is believed to be related to altered blood flow in cardiac embryogenesis leading to obstruction of the left side of the heart (Towbin *et al.* 1999). At least 10% of patients die within one week, and all patients without treatment die in the first year of life. HLHS is known to be occasionally associated with the following genetic entities: (i) Mendelian disorders: Apert syndrome, Holt-Oram syndrome, Ellis-van Creveld syndrome, Smith-Lemi-Opitz syndrome, Beckwith-Wiedemann syndrome, CHARGE syndrome, DiGeorge syndrome, Heterotaxy, Allagile syndrome, Rubinstein-Taybi syndrome, short rib-polydactyly syndrome type 3, PAGOD syndrome (Natowicz *et al.* 1988; Hanauer *et al.* 2002; Robert *et al.* 2007); (ii) Chromosomal abnormalities (including microdeletion syndromes): trisomy 13, trisomy 18, Turner syndrome, 7q35 deletion, Jacobsen syndrome and 16q24 deletion (Grossfeld 1999; Sedmera *et al.* 2005); and (iii) Non-Mendelian disorders: Sirenomelia sequence (Kim *et al.* 2007). However, a search of English-language publications failed to find any cases of Peters Plus syndrome associated with HLHS.

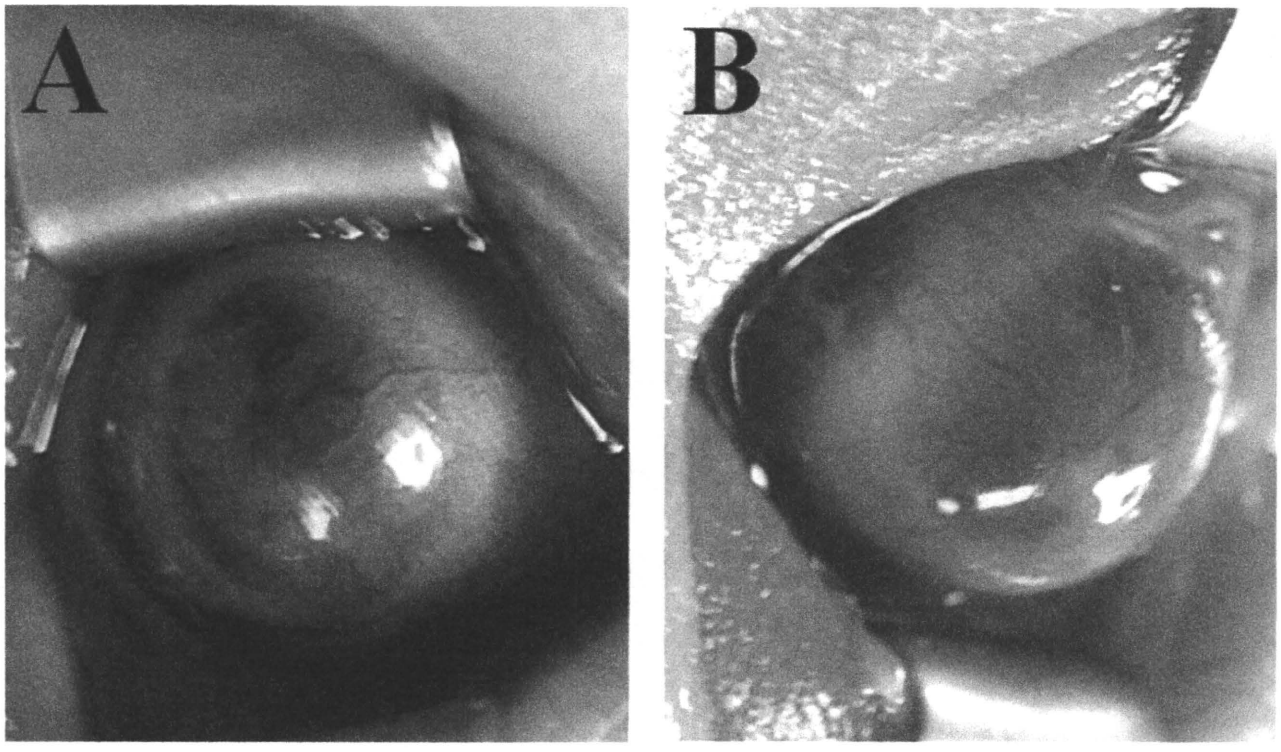

Fig. 2 Anterior staphyloma of both eyes. (A) Right eye. (B) Left eye.

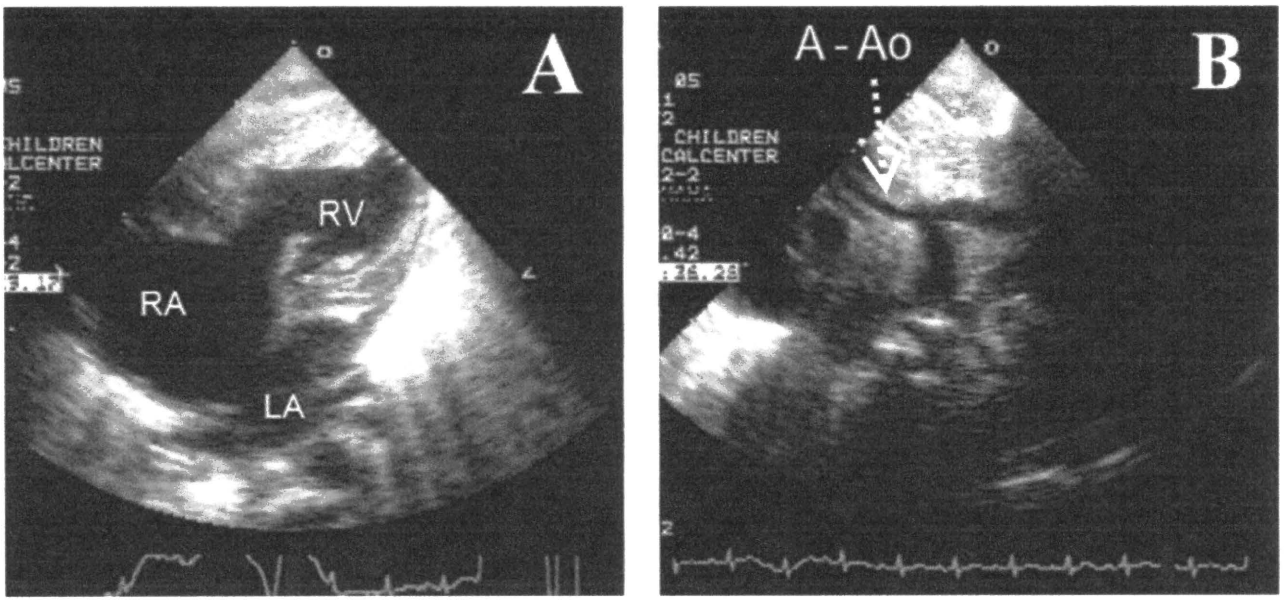

Fig. 3 Echocardiographic image of the patient. (A) Apical four-chamber view. Note hypoplastic left ventricle. (B) Suprasternal sagittal view. Note narrow ascending aorta of less than 1.5 mm in diameter. A-Ao, ascending aorta; LA, left atrium; RA, right atrium; RV, right ventricle.

Analysis of *B3GALTL* gene mutation status in two previous studies revealed the exclusively constant c.660 + 1G > A mutation in exon 8. Of 19 patients (or families) studied, homozygous c.660 + 1G > A mutation was found in 15 patients, and the remaining four patients were compound heterozygotes for the common c.660 + 1G > A mutation and for another mutation, c.230insT, c.347 + 5G > A, c.459 + 1C > A, and entire gene deletion, respectively (Lesnik Oberstein *et al.* 2006; Reis *et al.* 2008). It is noteworthy that mutations were found in all these typical patients.

The most characteristic feature of Peters Plus syndrome is Peters anomaly of the anterior eye chamber characterized by central corneal opacity (leukoma), thinning of the posterior aspect of the cornea, and iridocorneal adhesions, which are observed in 73% of patients (Maillette de Buy Wenniger-Prick and Hennekam 2002). The remaining patients have less severe anterior chamber manifestations, such as posterior embryotoxon. However, anterior staphyloma (ectasia of the cornea usually covered on the posterior surface by remnants of anteriorly displaced iris) present in our patient, a most severe expression of anterior chamber maldevelopment, is apparently rare in the syndrome.

As mentioned above, our patient showed unusual features of Peters Plus syndrome, such as HLHS and anterior staphyloma. Although we failed to identify similar previously published cases, an extensive search of non-English (Japanese) publications revealed a case similar to our patient. Nozaki *et al.* (1996) reported a 25-day -old Japanese boy who had anterior staphyloma in his left eye and HLHS. The cornea in his left eye was protruding and diffusely clouded and no recognizable anterior chamber structures were present, while hyperplasia of the iris stroma was noted in the right eye. Other features also described were congenital teeth, high arched palate, low-set ears and retained testes.

In conclusion, our patient and the patient reported by Nozaki *et al.* (1996) might represent a new syndrome of severe Peters Plus syndrome-like phenotype with anterior eye staphyloma and HLHS. The fact that no *B3GALTL* mutation was found in our patient also suggests this notion.

ACKNOWLEDGMENT

This work was partly sponsored by a grant from the Ministry of Health, Labour and Welfare, Japan.

REFERENCES

Grossfeld PD (1999) The genetics of hypoplastic left heart syndrome. *Cardiol Young* **9**: 627–632.

Hanauer D, Argilla M, Wallerstein R (2002) Rubinstein-Taybi syndrome and hypoplastic left heart. *Am J Med Genet* **112**: 109–111.

Kim JB, Park JJ, Ko JK *et al.* (2007) A case of PAGOD syndrome with hypoplastic left heart syndrome. *Int J Cardiol* **114**: 270–271.

Lesnik Oberstein SA, Kriek M, White SJ *et al.* (2006) Peters Plus syndrome is caused by mutations in B3GALTL, a putative glycosyltransferase. *Am J Hum Genet* **79**: 562–566.

Maillette de Buy Wenniger-Prick LJ, Hennekam RC (2002) The Peters' Plus syndrome: a review. *Ann Genet* **45**: 97–103.

Natowicz M, Chatten J, Clancy R *et al.* (1988) Genetic disorders and major extracardiac anomalies associated with the hypoplastic left heart syndrome. *Pediatrics* **82**: 698–706.

Nozaki M, Shirai S, Ozeki H, Majima A (1996) A case of Peters' anomaly with systemic malformations. *Rinsho Ganka* **50**: 1307–1311.

Reis LM, Tyler RC, Abdul-Rahman O *et al.* (2008) Mutation analysis of B3GALTL in Peters Plus syndrome. *Am J Med Genet A* **146A**: 2603–2610.

Robert ML, Lopez T, Crolla J *et al.* (2007) Alagille syndrome with deletion 20p12.2-p12.3 and hypoplastic left heart. *Clin Dysmorphol* **16**: 241–246.

van Schooneveld MJ, Delleman JW, Beemer FA, Bleeker-Wagemakers EM (1984) Peters' Plus: a new syndrome. *Ophthalmic Paediatr Genet* **4**: 141–145.

Sedmera D, Cook AC, Shirali G, McQuinn TC (2005) Current issues and perspectives in hypoplasia of the left heart. *Cardiol Young* **15**: 56–72.

Towbin JA, Casey B, Belmont J (1999) The molecular basis of vascular disorders. *Am J Hum Genet* **64**: 678–684.

Int J Oral-Med Sci 9(2):101-107, 2010

Original Article

A Comparison between Two-Dimensional and Three-Dimensional Cephalometry on Lateral Radiographs and Multi-Detector Row Computed Tomography of Human Skulls

Norimitsu Hirai,[1] Takahiro Yamauchi,[2] Kensuke Matsune,[2] Ryosuke Kobayashi,[1] Hitoshi Yabe,[3] Hirofumi Ohashi,[4] and Takahide Maeda[2]

[1]Nihon University Graduate School of Dentistry at Matsudo, Pediatric Dentistry, Matsudo, Chiba 271-8587, Japan
[2]Department of Pediatric Dentistry, Nihon University School of Dentistry at Matsudo, Matsudo, Chiba 271-8587, Japan
Divisions of [3]Radiology, and [4]Medical Genetics, Saitama Children's Medical Center, Iwatsuki, Saitama 339-8551, Japan

Correspondence to :
Norimitsu Hirai
E-mail : mano07011@g.nihon-u.ac.jp

Abstract

Proper understanding of the orofacial development and deformities associated with various syndromes is important for planning appropriate dental treatment and improving the craniofacial features. However, it is quite difficult to take cephalometric radiographs of patients with severe mental retardation or behavioral disorders, since patient co-operation and stability of body movement are necessary while taking the radiographs. Computed tomography (CT) is potentially a better tool for the diagnosis and treatment planning of complex maxillofacial deformities than conventional lateral cephalograms. CT images of patients with mental retardation can be taken under general anesthesia. The absorbed dose of radiation in 128 slice multi-detector row computed tomography (MDCT) used in this study is established as CTDI vol. 17.24 mGy, which is less than that of conventional CT (65 mGy). However, the use of MDCT for cephalometric analysis in pediatric dentistry has not been reported. Hence, the aim of the present study was to compare the reliability and difference of angle and linear measurements of craniofacial form using the landmarks on conventional and MDCT lateral cephalograms of human skulls. The results of this study showed that angular and linear measurements recorded from conventional and MDCT lateral cephalograms were similar. In conclusion, there were no significant differences in the mean and standard deviation of angular and linear measurements between conventional and MDCT lateral cephalograms of human skulls. Angular and linear analysis on MDCT cephalogram might show good precision for craniofacial analysis.

Keywords :
128 multi-detector row computed tomography, lateral cephalogram, angular analysis, linear analysis

Introduction

Since 1931, lateral cephalometric radiographs have been used for analyzing both maxillofacial and orthodontic deformities, and especially to evaluate growth in pediatric dentistry (1, 2). Proper understanding of the orofacial development and deformities associated with various syndromes is important for planning appropriate dental treatment and improving the craniofacial features. However, it is quite difficult to take cephalometric radiographs of patients with severe mental retardation or behavioral disorders, since patient co-operation and stability of body movement are necessary while taking the radiographs.

Computed tomography (CT) provides detailed information regarding the landmarks through sliced images. In modern medical CT, the x-ray source rotates within the gantry chamber that houses the x-ray tube and detector while the patient is being moved through the gantry on a bed ; this method of

CT scanning is known as helical CT and is the most widely used (3). CT, therefore, is potentially a better tool in the diagnosis and treatment planning of complex maxillofacial deformities than conventional cephalometrics (4). Furthermore, it is possible to take CT images of patients with mental retardation under general anesthesia.

Spiral CT, however, places a great biological burden on the patient because of its high radiation exposure. As radiation has a cumulative effect on the human body, any reduction in exposure to radiation is considered beneficial. With the recent introduction of cone-beam CT specifically designed for volumetric imaging of the maxillofacial area, the radiation dose to the patient is significantly reduced, which effectively reduces the exposure time and simultaneously reduces the absorbed radiation to the patient (5).

In recent years, cone beam CT technology has become more popular. Cone beam CT scan exposes the patient to less radiation than multi-detector row CT (6). The absorbed dose of x-ray in 128 multi-detector row computed tomography (MDCT) used in this study is established as CTDI vol. 17.24 mGy, which is less than that of conventional CT (65 mGy). Chest CT is the most sensitive diagnostic imaging modality for detection of lung cancer and the treatment of any equivocal abnormalities detected on chest radiographs (7, 8). With spiral CT and, more recently, multi-detector row CT techniques, the sensitivity for detection of lung cancer and pulmonary nodules has improved, and the best method of assessing tumor response in most clinical situations is MDCT, which can detect a large number of lesions with smaller diameters and has more precision on measuring when compared with other methods (9).

The craniofacial characteristics of many syndromes are still unknown because of the difficulty of obtaining stable images by conventional lateral cephalograms. CT is beneficial for patients who have craniofacial anomalies and orofacial clefts, or patients requiring orthognathic surgery. The use of MDCT for lateral cephalometric analysis has not been reported in pediatric dentistry. Therefore, the authors compared conventional and MDCT lateral cephalograms. To obtain accurate angle and linear data from two-dimensional images, positioning of the patient is of utmost importance, whereas positioning of the patient is not critical when recording three-dimensional images (10).

Hence, the aim of the present study was to compare the reliability and difference of angle and linear measurements of craniofacial form using the landmarks on conventional and MDCT lateral cephalograms of human skulls.

Materials and Methods

Six dry human skulls were obtained from the Department of Oral Anatomy, Nihon University School of Dentistry at Matsudo. In order to confirm the differences of linear and angle measurements in different developmental stages, skulls with three types of dentition were selected as follows: Phantom 1 with primary dentition, Phantoms 2 and 3 with mixed dentition, and Phantoms 4, 5 and 6 with permanent dentition. All skulls had normal occlusion and no deformity of craniofacial pattern. The mandibular position was fixed with adhesive tape from the ipsilateral temporal bone around the horizontal ramus of the mandible to the contralateral temporal bone.

Imaging protocol

Each phantom was positioned in the Cephalostat (AUTO III N CM: Asahi Roentogen) by fixing it between the ear rods. The ear rods were placed in the external acoustic meatus and the Frankfort horizontal plane was placed perpendicular to the floor. Lateral cephalograms were taken with the following radiographic settings, for all phantoms: 75 kV, 12 mA, 0.63 s. The phantoms were placed in MDCT of SOMATOM Definition AS+(SIEMENS) on a foam platform with the Frankfort horizontal plane perpendicular to the floor and the position of the center of SOMATOM was set using the midline light beam to coincide with the midsagittal plane. Six phantoms were scanned with MDCT, which acquires 128 slices per gantry rotation at a gantry rotation time of 500

ms. The imaging conditions of MDCT were as follows for all phantoms in the extended height mode : 120 kV ; 120 mAS ; resolution, 0.12~0.15 mm ; FOV, 180 mm~200 mm ; slice width, 38 mm ; helical pitch (H.P.), 1.2 mm ; exposure time, 4.18 s ; window width ; 1500 ; window level, 450 ; absorbed dose, CTDI vol. 17.24 mGy.

Lateral cephalometric radiographs

For the lateral cephalometric analysis, 19 landmarks with Frankfort plane based on the anatomical Porion were identified. Based on Down's analysis for Japanese, angle and linear measurements for phantoms with primary and mixed dentition, and permanent dentition were recorded on both images. On conventional cephalograms, the authors measured the angle between three landmarks using a protractor having a minimum unit of 0.5° and the linear dimensions between two landmarks using a 1/20 mm caliper. Each measurement was repeated three times. On MDCT images and conventional cephalograms, the same examiner marked 19 landmarks and measured angle and linear dimensions three times with a time interval of 1 day. All measured data in MDCT images were calculated by Syngo fastview (standalone viewing tool for DICOM images) software in each phantom. The identified cephalometric hard tissue landmarks were set by the same dentist who had 5 years clinical experience with conventional and MDCT lateral cephalograms. In the MDCT cephalograms, the linear values recorded were calculated as the data based on the scale bar in each image. In linear analysis of the conventional cephalograms, as the image was 1.1 times larger than the true measurement (11), the data obtained were divided by 1.1. Fig. 1 indicates the landmarks on conventional and MDCT cephalograms.

Statistical analysis

The mean value and standard deviation of angle and linear analyses in six phantoms on conventional and MDCT lateral cephalograms were statistically analyzed by Paired t-test.

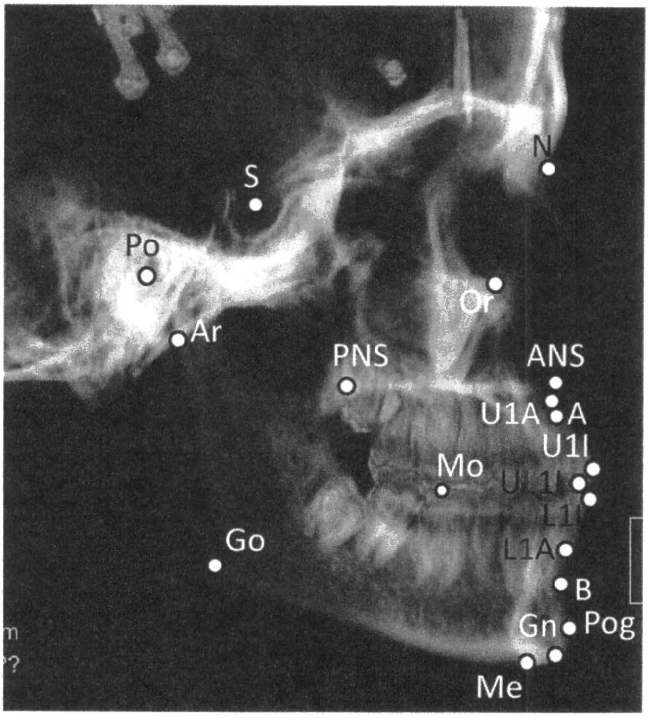

Fig. 1. Cephalometric image of MDCT

Results

In the present study, the intraobserver errors of angular analysis in conventional and MDCT lateral cephalograms (Fig. 1) were within 2.1 and 0.6° at Upper 1 to FH plane, respectively, on Phantom 1 with primary dentition (Table 1). On Phantom 6 with permanent dentition, the intraobserver errors were within 0.8° at FH to Upper 1 in both images (Table 2).

No significant differences in angular analysis were shown between conventional and MDCT cephalograms on Phantoms 1, 2, 3 with primary and mixed dentition. (Table 3), and Phantom 4, 5 and 6 with permanent dentition (Table 4).

The results of linear analysis of lateral cephalograms in conventional and MDCT images of Phantom 1 with primary dentition are shown in Table 5, and those of Phantom 6 with permanent dentition are indicated in Table 6. The intraobserver errors of linear analysis in two images were 0.1 mm to 0.4 mm on conventional and 0.1 mm on MDCT lateral cephalograms on Phantom 1, and were within 0.6 mm in both cephalograms on Phantom 6 (Tables 5 and 6).

Tables 7 and 8 show the average linear dimensions

Table 1. Angular analysis on conventional and MDCT cephalogram of Phantom 1 with primary dentition

	Conventional			MDCT		
Angular analysis	mean	SD	σi	mean	SD	σi
Skeletal						
Convexity	8.7	0.5	0.6	8.7	0.2	0.3
A-B plane	−5.8	0.2	0.3	−5.8	0.2	0.3
SNA	78.3	0.5	0.6	78.5	0.4	0.5
SNB	73.3	0.5	0.6	73.5	0.4	0.5
Facial angle	85.0	0.4	0.5	84.8	0.2	0.3
SNP	73.8	0.5	0.6	74.0	0.4	0.5
Y axis	58.2	0.2	0.3	58.3	0.2	0.3
SN-S·Gn	69.3	0.6	0.8	69.2	0.2	0.3
Mandibular plane	27.2	0.2	0.3	27.3	0.2	0.3
Gonial angle	127.2	0.2	0.3	127.3	0.2	0.3
GZN	90.3	0.2	0.3	90.2	0.2	0.3
FH to SN	11.2	0.5	0.6	11.0	0.0	0.0
Denture						
U-A to FH plane	100.7	1.7	2.1	100.7	0.5	0.6
U-A to SN plane	90.0	0.8	1.0	89.8	0.2	0.3
L-1 to Mandibular	81.5	1.5	1.8	81.7	0.5	0.6
Interincisal	150.5	0.4	0.5	150.3	0.5	0.6
Occlusal plane	9.7	0.9	1.2	9.8	0.2	0.3

SD; standard deviation, σi; intraobserver errors

Table 2. Angular analysis on conventional and MDCT cephalogram of Phantom 6 with permanent dentition

	Conventional			MDCT		
Angular analysis	mean	SD	σi	mean	SD	σi
SN to FH	13.8	0.2	0.3	14.0	0.4	0.5
SN to Palatal	10.8	0.2	0.3	11.0	0.4	0.5
SN to Mandibular	25.2	0.2	0.3	25.2	0.2	0.3
FH to Occlusal	6.2	0.2	0.3	6.2	0.2	0.3
FH to Mandibular	11.3	0.2	0.3	11.0	0.4	0.5
SNA	81.0	0.0	0.0	81.0	0.0	0.0
FH to NA	94.7	0.2	0.3	94.7	0.2	0.3
Convexity	−3.7	0.2	0.3	−3.8	0.2	0.3
SNB	82.0	0.0	0.0	82.2	0.2	0.3
SN Pog	82.5	0.0	0.0	82.8	0.2	0.3
FH to NB	95.8	0.2	0.3	95.7	0.2	0.3
Facial angle	96.8	0.2	0.3	97.0	0.0	0.0
Y axis	51.0	0.0	0.0	50.8	0.2	0.3
Gonial angle	112.5	0.4	0.5	112.8	0.2	0.3
ANB	−1.0	0.0	0.0	−1.2	0.2	0.3
Palatal to Mandibular	14.2	0.2	0.3	14.0	0.4	0.5
FH to Upper 1	125.0	0.4	0.5	125.2	0.6	0.8
FH to Lower 1	78.0	0.4	0.5	77.8	0.2	0.3
Interincisal	132.8	0.2	0.3	132.5	0.4	0.5
Mandibular to Lower 1	90.3	0.2	0.3	90.7	0.2	0.3

SD; standard deviation, σi; intraobserver errors

Table 3. Average of angular analysis on conventional and MDCT cephalograms of three phantoms with one primary and two mixed dentition

	Conventional		MDCT		
	mean	SD	mean	SD	*t*-test
Skeletal					
Convexity	11.7	2.1	11.6	2.1	1.0
A-B plane	−8.1	1.6	−8.3	1.9	0.9
SNA	79.3	1.7	79.8	1.6	0.8
SNB	73.1	0.9	73.4	0.7	0.7
Facial angle	82.8	2.1	82.7	2.2	1.0
SNP	73.6	0.9	73.8	0.8	0.8
Y axis	60.9	2.8	62.0	2.9	0.7
SN-S·Gn	70.3	1.5	70.2	1.4	0.9
Mandibular plane	29.0	4.0	29.9	3.7	0.8
Gonial angle	128.5	3.4	128.3	3.1	1.0
GZN	89.5	0.5	89.3	0.8	0.8
FH to SN	9.3	1.6	8.9	1.9	0.8
Denture					
U-1(A) to FH plane	100.8	7.8	100.4	8.2	1.0
U-1(A) to SN plane	92.2	8.5	92.2	8.8	1.0
L-1 to Mandibular	87.9	5.0	88.1	4.6	1.0
Interincisal	141.4	13.5	140.9	13.8	1.0
Occlusal plane	14.6	3.7	15.7	4.3	0.8

$p<0.05$ SD; standard deviation

Table 4. Average of angular analysis on conventional and MDCT cephalograms of three phantoms with permanent dentition

	Conventional		MDCT		
	mean	SD	mean	SD	*t*-test
SN to FH	11.4	1.8	11.1	2.1	0.9
SN to Palatal	9.5	2.0	9.1	2.3	0.8
SN to Mandibular	27.2	3.1	27.3	2.5	1.0
FH to Occlusal	6.7	0.7	6.6	0.8	0.8
FH to Mandibular	16.3	4.6	16.1	4.2	1.0
SNA	82.8	1.9	83.1	1.5	0.9
FH to NA	94.0	0.3	94.3	0.3	0.4
Convexity	6.1	7.1	5.9	7.0	1.0
SNB	79.7	1.8	79.8	1.8	1.0
SN Pog	80.5	1.5	80.7	1.7	0.9
FH to NB	90.8	3.4	90.9	3.5	1.0
Facial angle	91.7	3.3	92.1	3.6	0.9
Y axis	55.4	3.3	55.5	3.3	1.0
Gonial angle	115.9	9.6	116.1	8.9	1.0
ANB	3.1	3.7	3.4	3.3	0.9
Palatal to Mandibular	17.9	5.0	17.8	4.4	1.0
FH to Upper 1	116.9	6.3	116.9	5.9	1.0
FH to Lower 1	65.9	9.3	65.3	9.1	1.0
Interincisal	128.6	4.3	128.3	4.2	1.0
Mandibular to Lower 1	97.9	5.0	98.2	5.4	1.0

$p<0.05$ SD; standard deviation

Table 5. Linear analysis in conventional and MDCT cephalogram of Phantom 1 with primary dentition

	Conventional			MDCT		
	mean	SD	σi	mean	SD	σi
S-N	55.8	0.1	0.1	56.6	0.0	0.0
ANS-PNS	39.5	0.3	0.4	39.9	0.0	0.1
Go-Me	46.2	0.2	0.2	46.9	0.0	0.0
S-Go	48.9	0.1	0.1	48.8	0.1	0.1
N-Pog	79.6	0.1	0.2	79.8	0.1	0.1
Or-ANS	18.3	0.3	0.4	17.7	0.1	0.1

SD ; standard deviation, σi ; intraobserver errors

Table 6. Linear analysis on conventional and MDCT cephalogram of Phantom 6 with permanent dentition

	Conventional			MDCT		
	mean	SD	σi	mean	SD	σi
S-N	60.7	0.1	0.2	60.2	0.0	0.3
ANS-PNS	47.0	0.2	0.2	46.2	0.6	0.6
Go-Me	68.6	0.2	0.3	68.1	0.0	0.1
S-Go	68.9	0.1	0.1	69.3	0.1	0.2
N-Pog	94.7	0.1	0.1	94.2	0.2	0.2
Or-ANS	23.7	0.1	0.1	23.3	0.4	0.2

SD ; standard deviation, σi ; intraobserver errors

Table 7. Average of linear analysis on conventional and MDCT cephalograms of three phantoms with one primary and two mixed dentition

	Conventional		MDCT		
	mean	SD	mean	SD	*t*-test
S-N	57.4	4.3	57.7	4.2	0.9
ANS-PNS	40.2	3.7	40.8	3.8	0.9
Go-Me	50.0	4.5	49.7	3.7	0.9
S-Go	53.0	4.5	52.5	4.3	0.9
N-Pog	84.4	9.3	84.7	9.2	1.0
Or-ANS	19.4	2.4	19.4	2.5	1.0

$p<0.05$ SD ; standard deviation

Table 8. Average of linear analysis on conventional and MDCT cephalograms of three phantoms with permanent dentition

	Conventional		MDCT		
	mean	SD	mean	SD	*t*-test
S-N	61.6	0.9	61.8	1.5	0.9
ANS-PNS	49.9	3.1	50.0	4.0	1.0
Go-Me	65.1	7.5	64.6	7.1	0.9
S-Go	69.3	5.0	69.7	5.0	0.9
N-Pog	96.6	3.4	96.4	4.0	1.0
Or-ANS	26.4	3.6	26.6	4.0	0.9

$p<0.05$ SD ; standard deviation

in conventional and MDCT lateral cephalograms in primary/mixed dentition and permanent dentition, respectively. The mean and standard deviation of linear dimensions in primary/mixed dentition and permanent dentition in conventional and MDCT lateral cephalograms were similar, and showed no significant difference.

Discussion

Recently, the application of three-dimensional (3D) lateral CT images is becoming more popular in the field of pediatric dentistry. Especially in mentally retarded patients, it is difficult to take conventional two-dimensional (2D) lateral and frontal cephalograms. However, evaluation of craniofacial development and symmetry is necessary to determine the craniofacial characteristics and plan appropriate treatment. Regardless of the type of CT used, the images produced by CT method allow better localization of the anatomical structures than conventional 2D radiographs, which are often geometrically distorted and plagued by bilateral structural superimpositions (12). Van Vlijmen *et al.* (13) reported that the position of the patient plays an important role in the outcome of cephalometric analysis because the measurements are influenced by tilt or rotations of the head. The position of the patient in CT scanner is not that important for 3D angular and linear measurements because rotation along the long axis or the sagittal axis is not of any influence. CT is potentially a better tool for the diagnosis and treatment planning of the complex maxillofacial deformities than conventional cephalograms (14).

Spiral CT, however, places a high economic and biological burden on the patient because of its high cost and radiation exposure. As radiation has a cumulative effect on the human body, any reduction in exposure to radiation is considered beneficial. The

new MDCT reduces exposure time and simultaneously reduces the radiation absorbed by the patient (15, 16). The MDCT-derived 3D cephalogram has a number of potential advantages over conventional CT, including sub-millimeter resolution and reduced radiation exposure, while still permitting reconstruction of the soft tissue profile. However, landmarks should be marked accurately on images for cephalometric analysis. In some cases, it is quite difficult to locate the landmarks, thus leading to an incorrect diagnosis. The main reason for errors in cephalometric studies is errors in landmark identification (17). Landmark identification is essential not only on conventional but also on MDCT lateral cephalograms. Williams and Richtsmeier (18) studied the reliability of 28 skeletal mandibular landmarks and the accuracy of 378 linear distances formed by the landmarks on 3D spiral CT images, and the mean accuracy of all linear distances was 0.377 ± 1.136 mm with a range of 0.001 to 3.889 mm, and approximately 58% of measurements were less than 1.0 mm from true values. They concluded that MDCT proved to be slightly more accurate than cone beam CT. Lou *et al.* (14) reported that for the conventional landmarks used in lateral and frontal cephalograms, there was no evidence to indicate that 3D spiral CT was more reliable than cephalometric methods. They stated that 3D CT should be reserved for severe asymmetric craniofacial cases. In a study by Mischkowski *et al.* (19), 30 holes with a diameter of 0.6 mm were drilled with a surgical drill in defined positions in the maxillofacial area of a dry human skull and all distances were measured manually with a precision digital caliper. They compared these values with measurements recorded by cone-beam CT (CBCT) and MDCT. The authors concluded that linear distance measurements revealed an average absolute error of 0.26 ± 0.18 mm for CBCT scanner and of 0.18 ± 0.17 mm for the MDCT scanner, which were not statistically significant. Slight differences of some of the linear measurements on conventional and MDCT lateral cephalograms were observed, however, which were similar to those reported by Cavalcanti *et al.* (20). This difference was most likely due to the discord between 2D and 3D images in which landmarks were identified. However, these differences probably do not translate into clinical relevance.

In the present study, the intraobserver errors of angular and linear analysis in conventional and MDCT lateral cephalograms were small in primary, mixed and permanent dentitions. The difference of angular and linear analysis between conventional and MDCT cephalograms was not significant.

From this study, it is suggested that MDCT cephalograms might be clinically accurate for craniofacial analyses.

Conclusion

Angular and linear measurements in conventional and MDCT lateral cephalograms were similar. The differences of data in each angular and linear measurement between conventional and MDCT cephalometry were within an angle of 1.1° and a length of 0.6 mm, respectively.

In conclusion, no significant differences were found in the mean and standard deviation of angular and linear measurements between conventional and MDCT lateral cephalograms in six skulls. The angular and linear analysis on MDCT cephalograms might be clinically accurate for craniofacial analysis.

Acknowledgments

The authors would like to thank Prof. T. Kaneda, Department of Radiology, for his valuable advice and Prof. E. Kanazawa, Department of Anatomy and Physical Anthropology, for his continuous and kind support.

This study was funded in part by a Grant for the Support of Projects for Strategic Research at Private Universities by the Ministry of Education, Culture, Sports, Science and Technology (MEXT), 2008-2012.

References

1. Broadbent BH : A new technique and its application to orthodontia. Angle Orthod, 1 : 45-66, 1931.
2. Gottlieb EL, Nelson AH, Vogels DS : 1990 JCO study

of orthodontic diagnosis and treatment procedures 1 Results and trends. J Clin Orthod, 25 : 145-156, 1991.
3. Hounsfield GN : Computerized transverse axis scanning (tomography) Part 1 Description of system. Br J Radiol, 68 : 166-172, 1995.
4. Carlsson CA : Imaging modalities in x-ray computerized tomography and in selected volume tomography. Phy Med Bio, 44 : 23-56, 1999.
5. Mah JK, Danforth RA, Bumann A, Hatcher D : Radiation absorbed in maxillofacial imaging with a new dental computed tomography device. Oral Surg Oral Med Oral Pathol Oral Radiol Endod, 96 : 508-513, 2003.
6. Ludlow JB, Ivanovic M : Comparative dosimetry of dental CBCT devices and 64-slice CT for oral and maxillofacial radiology. Oral Surg Oral Med Oral Pathol Oral Radiol Endod, 106 : 106-114, 2008.
7. Heitzman ER : The role of computed tomography in the diagnosis and management of lung cancer, an overview. Chest, 89 : 237-241, 1986.
8. Henschke CI, McCauley DI, Yankelevitz DF, Naidich DP, McGuinness G, Miettinen OS, Libby DM, Pasmantier MW, Koizumi J, Altorki NK, Smith JP : Early Lung Cancer Action Project : overall design and findings from baseline screening. Lancet, 354 : 99-105, 1999.
9. Erasmus JJ, Gladish GW, Broemeling L, Sabloff BS, Truong MT, Herbst RS, Munden RF : Interobserver and intraobserver variability in measurement of non-small-cell carcinoma lung lesions : implications for assessment of tumor response. J Clin Oncol, 21 : 2574-2582, 2003.
10. Swennen GRJ, Schutyser F, Hausamen JE, eds : Three dimensional cephalometry. A color atlas and manual. Berlin : Heidelberg Springer, 183-226, 2005.
11. Sebata M, Yamaguchi H : Morphological examination. In : Iizuka T, Sebata M, Iwasawa T, Motohashi Y. Orthodontics. Ishiyaku Shuppan ; 1992. p.169-171.
12. Salzmann JA : Limitation of roentgenographic cephalometrics. Am J Orthod, 50 : 169-188, 1964.
13. van Vlijmen OJ, Maal T, Bergé SJ, Bronkhorst EM, Katsaros C, Kuijpers-Jagtman AM : Comparison of cephalometric radiographs obtained from cone beam computed tomography scan and conventional radiographs. J Oral Maxillofac Surg, 67 : 92-97, 2009.
14. Lou L, Lagravere MO, Compton S, Major PW, Flores-Mir C : Accuracy of measurements and reliability of landmark identification with computed tomography (CT) techniques in the maxillofacial area : a systematic review. Oral Surg Oral Med Oral Pathol Oral Radiol Endod, 104 : 402-411, 2007.
15. Mozzo P, Procacci C, Tacconi A, Martini PT, Andreis IA : A new volumetric CT machine for dental imaging based on the cone-beam technique : preliminary results. Eur Radiol, 8 : 1558-1564, 1998.
16. Mah JK, Danforth RA, Bumann A : Radiation absorbed in maxillofacial imaging with a new dental computed tomography device. Oral Surg Oral Med Oral Pathol Oral Radiol Endod, 96 : 508-513, 2003.
17. Houston WJ : The analysis of errors in orthodontic measurements. Am J Orthod, 83 : 382-390, 1983.
18. Williams FL, Richtsmeier JT : Comparison of mandibular landmarks from computed tomography and 3D digitizer data. Clin Anat, 16 : 494-500, 2003.
19. Mischkowski RA, Pulsfort R, Ritter L, Neugebauer J, Brochhagen HG, Keeve E, Zöller JE : Geometric accuracy of a newly developed cone-beam device for maxillofacial imaging. Oral Surg Oral Med Oral Pathol Oral Radiol Endod, 104 : 551-559, 2007.
20. Cavalcanti MG, Vannier MW : Three dimensional computed tomography landmark measurement in craniofacial surgical planning : experimental validation in vitro. J Oral Maxillofac Surg, 57 : 690-694, 1999.

Int J Oral-Med Sci 9(2):108-114, 2010

Original Article

Accuracy of Tooth Development Stage, Tooth Size and Dental Arch width in Multi-Detector Row Computed Tomography of Human Skulls

Takahiro Yamauchi,[1] Norimitsu Hirai,[2] Kensuke Matsune,[1] Ryosuke Kobayashi,[2] Hitoshi Yabe,[3] Yasuo Takahashi,[4] Hirofumi Ohashi,[5] and Takahide Maeda[2]

[1]Department of Pediatric Dentistry, Nihon University School of Dentistry at Matsudo, Matsudo, Chiba 271-8587, Japan
[2]Nihon University Graduate School of Dentistry at Matsudo, Pediatric Dentistry, Matsudo, Chiba 271-8587, Japan
Divisions of [3]Radiology, [4]Pediatric Dentistry, and [5]Medical Genetics, Saitama Children's Medical Center, Iwatsuki, Saitama 339-8551, Japan

Correspondence to :
Norimitsu Hirai
E-mail : mano07011@g.nihon-u.ac.jp

Keywords :
128 multi-detector row computed tomography, tooth development stage, tooth size, dental arch width

Abstract
In pediatric dentistry, examination of the development of crown or tooth root is essential to determine the physiological development age. Measurements of the tooth size and dental arch width are also required to predict normal occlusion and oral function, and to plan appropriate dental treatment. Some dental anomalies are keys to identify congenital malformation syndromes. In patients with behavioral disorders, it is quite difficult to take diagnostic dental models and pantomographs, since patient co-operation and stability in body movement for a few minutes is necessary while taking the dental impression and pantomographs. For patients with severe mental retardation and behavioral disorders, performing computed tomography under general anesthesia or deep sedation is easier than taking pantomographs while awake. The aim of the present study was to compare the tooth development stage on pantomographs and mesiodistal diameter measurements of tooth size and dental arch width of dry human skulls with the images of those on 128 multi-detector row computed tomography (MDCT). Based on the results, the measurements of tooth development stage, tooth size and dental arch width on MDCT images were clinically precise.

Introduction

In pediatric dentistry, examination of the tooth development is essential to determine the physiological development age (1, 2). Measurements of tooth size and dental arch width are also required to predict normal occlusion (3) and oral function, and to plan appropriate dental treatment. Some dental anomalies are keys to identify congenital malformation syndromes (4). For thorough examination, dental models and pantomographs are necessary. To evaluate the craniofacial growth in children, lateral cephalometry (5) and pantomography (6) have been utilized. Tooth size anomalies like macrodontia or microdontia, abnormalities in teeth numbers and dental arch width with narrowed arch or high arched palatal vault are important in the detection of some syndromes. However, in some patients with behavioral disorders, taking diagnostic dental models and pantomographs is quite difficult, since the patient must co-operate and remain stable for a few minutes while taking the dental impression and pantomographs. In these patients, taking a dental impression involves the risk of apnea. For patients with severe mental retardation and severe behavioral disorder, performing computed tomography (CT) under general anesthesia or deep sedation is easier than taking pantomographs while awake.

A medical CT system known as multi-detector row computed tomography has recently been developed and is now being applied for the diagnosis of tumors (7), external injuries (8) and in the dental field for clarifying the relationship between the lower

third molar and inferior canal (9). In comparison with conventional CT systems, multi-detector row CT allows rapid imaging with a smaller burden on the patient, and yields higher image quality while requiring a small exposure dose (10, 11).

In recent years, up-to-date CT technology including cone beam CT with less radiation than conventional CT has been increasing in popularity. Recently, the 128 multi-detector row computed tomography (MDCT) used in the present study gained attention, because the CT provides detailed and accurate three-dimensional construction images with less radiation than conventional CT. The best method of assessing tumor response in most clinical situations is MDCT, as it can detect a large number of lesions with smaller diameters and measurement is more precise when compared with other methods (12). No study has compared the tooth development stage on conventional and MDCT pantomographs, and the tooth size and dental arch size on the skull and on the MDCT.

Hence, the aim of the study was to compare the tooth development stage of permanent teeth on pantomographs and mesiodistal diameter measurements of tooth size and dental arch width on the skull with MDCT images.

Materials and Methods

Six dry human skulls were obtained from the collection of the Department of Oral Anatomy and Physical Anthropology of Nihon University School of Dentistry at Matsudo. One skull (Phantom 1) with primary dentition, 2 skulls (Phantom 2 and Phantom 3) with mixed dentition and 3 skulls (Phantom 4, Phantom 5 and Phantom 6) with permanent dentition were used to estimate the tooth development of permanent teeth, and to measure the mesiodistal diameter of tooth size and dental arch width in primary, mixed and permanent dentitions. The mandibular position of phantoms was fixed with broad tape from the ipsilateral temporal bone around the horizontal ramus of the mandible to the contralateral temporal bone.

Imaging protocol

Each phantom was positioned in the cephalostat (AUTO IIIN CM: Ashahi Roentogen) by fixing it between the ear rods. The ear rods were placed in the external acoustic meatus and the Frankfort horizontal plane was placed perpendicular to the floor. For all phantoms, pantomographs were taken with the following radiographic settings: 75 kV, 12 mA, 0.63 s. The same phantoms were placed in MDCT of SOMATOM Definition AS+ (SIEMENS) on a foam platform with the Frankfort horizontal plane perpendicular to the floor and the position of the center of SOMATOM was set using the midline light beam to coincide with the midsagittal plane. The following imaging conditions were maintained for all phantoms in the extended height mode: 120 kV; 120 mAS; resolution, 0.12~0.15 mm; FOV, 180 mm ~200 mm; slice width, 38 mm; helical pitch (HP), 1.2 mm; exposure time, 4.18 s; window width, 1500; and window level, 450.

Tooth developmental stage

Based on the criteria of Nolla (1), the developmental stage of each permanent tooth was evaluated on conventional and MDCT pantomographs using a set of drawings illustrating the 10 stages of the teeth by a pedodontist who had over 5 years of clinical experience.

Tooth size and dental arch width

Crown mesiodistal diameter and dental arch width were directly measured on the six phantoms three times using a 1/20 mm caliper by the same observer. Dental arch width was expressed as Wc and We which means the distance between the most distal corners of the left-right primary canines and primary second molars, respectively, and W3 and W6 means the distance between the most distal corners of left-right permanent canines and permanent first molars, respectively.

On MDCT images, one dentist evaluated the most mesial and distal corners of each tooth, and Wc, We, W3 and W6 were measured three times. All data were calculated by Syngo fastview (standalone view-

ing tool for DICOM images) software in each phantom. In MDCT images, crown mesiodistal diameters and dental arch widths were measured from converted data based on the scale bar which was calculated and fixed as a true distance in each image.

Statistical analysis

From the conventional and MDCT pantomographs, one dentist evaluated the tooth developmental stage and measured crown diameter and dental arch width three times with a time interval of 1 day. The data of tooth development stage on conventional and MDCT pantomographs were statistically compared by Wilcoxon rank sum test, and tooth size and dental arch width were analyzed by paired t-test.

Results

Tooth development stage

Comparison of the tooth developmental stage of each permanent tooth on conventional and MDCT pantomographs of Phantom 1 is shown in Table 1 and Fig. 1. The difference of the average intraobserver errors of tooth development stage on conventional and MDCT pantomographs of Phantom 1 was 0.3. Data from Phantoms 2 and 3 are not shown, because those phantoms were very similar to Phantom 1. The average tooth development stages of permanent teeth in maxilla on the MDCT pantomographs in Phantoms 1, 2 and 3 were significantly higher than those of conventional pantomographs ($P<0.05$). No significant difference, however, was seen the average stages of the teeth in mandible between conventional and MDCT pantomographs in Table 2.

Fig. 1. Tooth development stage of permanent teeth by MDCT Pantomograph

Tooth size and dental arch width

Mesiodistal diameters of each primary tooth and

Table 1. Tooth development stage in pantomograph and MDCT of Phantom 1 with primary dentition

	mean(RU)	SD	σi	mean(LU)	SD	σi	mean(RL)	SD	σi	mean(LL)	SD	σi
pantomograph												
1	5.0	0.0	0.0	5.0	0.0	0.0	6.0	0.0	0.0	6.0	0.0	0.0
2	4.7	0.5	0.6	4.7	0.5	0.6	5.7	0.5	0.6	5.7	0.5	0.6
3	4.3	0.5	0.6	4.3	0.5	0.6	4.3	0.5	0.6	4.3	0.5	0.6
4	2.0	0.8	1.0	2.0	0.8	1.0	3.5	0.0	0.0	3.5	0.0	0.0
5	2.0	0.0	0.0	2.0	0.0	0.0	2.0	0.0	0.0	2.0	0.0	0.0
6	4.7	0.5	0.6	5.0	0.0	0.0	5.7	0.5	0.6	5.3	0.5	0.6
7	0.0	0.0	0.0	0.3	0.5	0.6	1.0	0.0	0.0	2.0	0.0	0.0
CT												
1	5.7	0.5	0.6	5.7	0.5	0.6	7.2	0.0	0.0	7.2	0.0	0.0
2	5.7	0.5	0.6	5.7	0.5	0.6	7.2	0.0	0.0	7.2	0.0	0.0
3	4.7	0.5	0.6	4.7	0.5	0.6	6.0	0.0	0.0	6.0	0.0	0.0
4	4.0	0.0	0.0	4.0	0.0	0.0	4.3	0.5	0.6	4.3	0.5	0.6
5	2.7	0.5	0.6	2.7	0.5	0.6	2.7	0.5	0.6	2.7	0.5	0.6
6	6.0	0.0	0.0	6.0	0.0	0.0	6.0	0.0	0.0	6.0	0.0	0.0
7	1.0	0.0	0.0	1.0	0.0	0.0	1.0	0.0	0.0	3.0	0.0	0.0

RU ; Right upper, LU : Left upper, RL : Right lower, LL : Left lower SD ; standard deviation, σi ; intraobserver errors

Table 2. Tooth development stages of upper and lower central incisor to second premolar in phantom and CT findings

	pantomograph			CT	
	mean	SD		mean	SD
Upper(1-5)	5.42	2.19	*	6.33	1.84
Lower(1-5)	6.06	2.01	NS	6.81	1.88

* ; $P<0.05$
NS ; not significant

Table 3. Tooth size in the skull and MDCT of Phantom 1 with primary dentition

		Skull			CT		
	teeth	mean	SD	σi	mean	SD	σi
Right Upper	A	6.3	0.0	0.0	6.2	0.0	0.1
	B	5.0	0.1	0.1	5.0	0.1	0.1
	C	6.3	0.2	0.2	6.3	0.0	0.1
	D	6.5	0.1	0.1	6.3	0.3	0.4
	E	8.4	0.1	0.1	8.3	0.1	0.2
Right Lower	A	3.7	0.0	0.0	3.8	0.3	0.4
	B	4.2	0.1	0.1	4.4	0.2	0.3
	C	5.6	0.0	0.0	5.6	0.0	0.1
	D	8.0	0.0	0.0	7.9	0.2	0.3
	E	9.5	0.5	0.6	9.5	0.2	0.2

SD ; standard deviation, σi ; intraobserver eerors

Table 4. Tooth size in the skull and MDCT of Phantom 6 with permanent dentition

		Skull			CT		
	teeth	mean	SD	σi	mean	SD	σi
Right Upper	1	9.0	0.1	0.1	8.8	0.1	0.1
	2	7.3	0.0	0.0	7.2	0.2	0.2
	3	7.8	0.0	0.0	7.8	0.1	0.1
	4	6.3	0.1	0.1	6.2	0.2	0.2
	5	5.8	0.1	0.1	5.7	0.0	0.1
	6	10.2	0.2	0.2	10.0	0.4	0.6
	7	9.3	0.1	0.2	8.7	0.1	0.2
Right Lower	1	5.7	0.0	0.0	5.5	0.1	0.2
	2	6.6	0.0	0.0	6.6	0.1	0.2
	3	6.9	0.1	0.1	6.9	0.2	0.2
	4	6.4	0.1	0.1	6.3	0.2	0.3
	5	6.6	0.0	0.0	6.5	0.4	0.5
	6	10.6	0.1	0.2	10.7	0.2	0.2
	7	9.9	0.0	0.0	10.4	0.1	0.2

SD ; standard deviation, σi ; intraobserver errors

permanent tooth on Phantom 1 and Phantom 6 on their MDCT images are shown in Table 3 and Table 4, respectively. Phantoms 2, 3, 4 and 5 are not shown. The intraobserver errors of tooth size on phantoms and MDCT images of Phantom 1 and Phantom 6 were limited within 0.6 mm, and dental arch widths of Wc, W_E, W3 W6 were within 0.4 mm, 0.3, 0.3 and 0.2, respectively. The tooth size and dental arch

Table 5. Average of tooth size in the Skull and MDCT of 6 phantoms

	Skulls		CT			Skulls		CT		
tooth	mean(RU)	SD	mean(RU)	SD	t-test	mean(RL)	SD	mean(RL)	SD	t-test
1	8.6	0.3	8.6	0.3	0.9	5.1	0.3	5.2	0.3	0.7
2	6.5	0.5	6.6	0.5	0.7	5.6	0.7	5.6	0.7	0.9
3	7.4	0.4	7.4	0.3	1.0	6.4	0.4	6.5	0.4	0.8
4	6.1	0.2	6.3	0.2	0.3	6.4	0.2	6.5	0.1	0.5
5	5.9	0.6	5.9	0.6	0.9	6.4	0.4	6.4	0.3	0.8
6	10.1	0.4	10.3	0.3	0.1	10.6	0.2	10.7	0.2	0.4
7	9.7	0.6	9.6	0.6	0.7	10.0	0.5	9.7	0.5	0.2
8	8.7	0.6	8.7	0.6	0.9	10.0	0.4	10.1	0.4	0.9
A	6.2	0.0	6.2	0.2	0.4	3.9	0.3	3.9	0.2	0.8
B	5.0	0.1	4.9	0.1	0.5	4.5	0.2	4.4	0.2	0.3
C	6.6	0.4	6.7	0.4	0.9	5.8	0.2	5.9	0.2	0.7
D	6.4	0.4	6.3	0.5	0.5	7.9	0.2	7.9	0.1	0.3
E	8.7	0.7	9.0	0.5	0.4	9.8	0.5	9.8	0.6	0.7

RU ; Right upper, RL ; Right lower $p<0.05$ SD ; standard deviation

Table 6. Dental arch width in Skull and MDCT of Phantom 1 with primary dentition

	Skull			CT		
	mean	SD	σi	mean	SD	σi
Upper Wc	31.1	0.2	0.2	31.0	0.1	0.2
WE	42.3	0.2	0.3	42.8	0.1	0.2
Lower Wc	25.2	0.1	0.1	24.9	0.3	0.4
WE	41.0	0.2	0.2	41.6	0.2	0.3

SD ; standard deviation, σi ; intraobserver errors

Table 7. Dental arch width in Skull and MDCT of Phantom 6 with permanent dentition

	Skull			CT		
	mean	SD	σi	mean	SD	σi
Upper W3	40.3	0.0	0.1	40.3	0.1	0.2
W6	57.9	0.1	0.1	57.7	0.1	0.2
Lower W3	31.7	0.1	0.1	31.5	0.3	0.3
W6	54.6	0.0	0.1	54.3	0.1	0.2

SD ; standard deviation, σi ; intraobserver errors

Table 8. Average of dental arch width in Skulls and MDCTs of primary and mixed dentition

	Skulls		CT		
	mean	SD	mean	SD	*t*-test
Upper Wc	33.9	3.7	34.3	4.0	0.9
WE	49.3	5.8	49.6	5.9	1.0
Lower Wc	27.4	2.6	27.7	3.0	0.9
WE	48.4	5.5	48.8	5.4	0.9

$p<0.05$ SD ; standard deviation

Table 9. Average of dental arch width in Skulls and MDCTs of permanent dentition

	Skulls		CT		
	mean	SD	mean	SD	*t*-test
Upper W3	39.3	1.5	39.4	1.3	0.9
W6	58.0	0.1	58.2	0.4	0.4
Lower W3	30.3	1.0	30.1	1.0	0.9
W6	52.9	1.6	53.0	1.6	1.0

$p<0.05$ SD ; standard deviation

width in phantoms and MDCT images were very similar. Table 5 shows the average mesiodistal diameter measurements of primary teeth and permanent teeth of the six phantoms. The differences of the mean mesiodistal diameter in upper and lower primary and permanent teeth between phantoms and MDCT images were less than 0.3 mm. Comparison of dental arch width on skull and MDCT images of Phantom 1 are shown in Table 6. Table 7 shows the mean dental arch width on phantom and MDCT images of Phantom 6. The average differences of the measurement of WC and WE in primary and mixed dentitions were within 0.4 mm (Table 8), and W3 and W6 on the six phantoms and MDCT images were less than 0.2 mm (Table 9). No significant differences were noted between them.

Discussion

In pediatric dentistry, determination of the physiological age and dental characteristics of child patients is essential to predict adult occlusion and proper dental treatment. Minor anomalies mostly occur in the craniofacial and oral regions. CT images are employed for diagnosis of some syndromes with mental retardation. Craniosynostosis is seen frequently in Apert, Crouzon and carpenter syndromes, delayed closure of fontanels is frequently seen in cleidocranial dysostosis and Down, Hallermann-Strief and Russell-Silver syndromes, maxillary hypoplasia with narrow and high arched palate are seen frequently in Crouzon, Marfan and Sotos syndromes, prognathism is seen frequently in Angelman, Gorlin and Sotos syndromes, micrognathia is seen frequently in Pierre Robin sequence and de Lange and Treacher-Collins syndromes, anodontia is seen frequently in ectodermal dysplasia and Ectrodactyly-ectodermal dysplasia-clefting syndrome (EEC), late eruption of teeth is seen frequently in cleidocranial dysostosis, de Lange syndromes and X-linked hypophosphatemic rickets, and microdontia is seen frequently in Down syndrome and ectodermal dysplasia. CT images are able to reveal the above anomalies in some syndromes with mental retardation (4).

In this study, the physiological age based on the development of permanent teeth was defined by the stages of Nolla (1), who discussed the development of permanent teeth at each physical age using a set of

drawings illustrating the 10 stages of the teeth as observed radiographically. In addition, Nolla noted that in order to obtain an appraisal of the development of a particular tooth, the radiograph was matched as closely as possible with the comparative figure. When the radiographic reading lay between two grades, this appraisal was indicated with a value of 0.5. For example, if between one-third and two-third of the tooth formation was completed, the reading of the radiograph was given a value of 7.5. When the radiographic value was slightly greater than the illustrated grade, but not as much as half way between that stage and the next, the value 0.2 was added. For example, if slightly more than two-thirds of the crown were completed it would become 4.2, or if somewhat more than one-third of the tooth were completed the grade would become 7.2. In the present study, the authors used Nolla's criteria and the development stages of each permanent tooth in only maxilla on MDCT pantomographs were scored slightly higher than the conventional pantomographs. MDCT pantomographs were clearer at the apical part of permanent teeth than conventional pantomographs, because MDCT pantomographs can confirm the tooth apex by the image in each slice. With regards the difference between maxilla and mandible, the authors considered that the permanent germs in maxilla were complexly located within thick bone, the positions of those germs, however, in mandible were located within thin bone.

Mesiodistal diameter of the crown in each primary and permanent tooth, and upper and lower dental arch widths in MDCT images were close to the corresponding values on the phantom. As the reliabilities of the tooth size and dental arch width measurements on MDCT and on phantom were both high, there were no significant differences in the mean and standard deviation of tooth size and dental arch width between MDCT images and the six phantoms. The measurements of tooth size and dental arch width on MDCT were sufficiently precise for dental structure analyses.

However, helical CT places a high economic and biological burden on the patient because of its high cost and high radiation exposure. As radiation has a cumulative effect on the human body, any reduction in exposure to radiation is considered beneficial. A newly developed type of CT reduces exposure time and simultaneously the absorbed radiation to the patient (13, 14), and MDCT exhibits more reduction of exposure.

Accurate landmarks should be put on images for mesiodistal diameter measurement. In some cases, it was quite difficult to identify the position of the landmark ; however, the mean value was similar to the tooth size on the phantom. The diagnosis of microdontia, macrodontia and abnormality of tooth morphology was reliable in the MDCT images. It was found that the measurements of tooth size and dental arch width on MDCT image were not significantly different from phantom measurements. A slight difference between MDCT data and phantom data does not translate into clinical relevance. The significant differences in this study were similar in magnitude to those of Cavalcanti *et al.* (15), who used cone beam CT. In the present study, most data regarding tooth development stage in each permanent tooth on MDCT pantomographs were significantly larger than those of conventional pantomographs. This finding suggested that the CT pantomograph was clearer and it showed more detail than conventional pantomographs. When MDCT pantomograph is used to evaluate tooth development age in clinics, clinicians have to consider the disagreement from Nolla criteria which based on conventional pantomograph. From this study, it was found that the tooth development stage on MDCT pantomographs was significantly earlier than that on conventional pantomographs, and tooth size and dental arch width on MDCT were similar to those of direct measurement on phantoms using a 1/20 mm caliper.

Conclusion

In this study, the average intraobserver error of tooth development stages in 56 permanent teeth was 0.3, and that of tooth size and dental arch widths on phantoms and MDCT was within 0.6 mm. The tooth

development stages in all permanent teeth were evaluated using conventional and MDCT pantomographs of dry human skulls, and the data of MDCT panoramagraphs were slightly higher than that of conventional pantomographs in only maxilla. The average differences in the mesiodistal diameters of all teeth and dental arch widths between phantoms and MDCT images were less than 0.3 mm, which was not significant.

From this study, the tooth development stage, tooth mesiodistal diameter and dental arch width analyses on MDCT image were found to be clinically precise.

Acknowledgments

The authors are grateful to Prof. T. Kaneda of the Department of Radiology in Nihon University School of Dentistry at Matsudo, valuable advice and Prof. E. Kanazawa of the Department of Anatomy and Physical Anthropology in Nihon University School of Dentistry at Matsudo, for his continuous and kind support.

This study was funded in part by a Grant for the Support of Projects for Strategic Research at Private Universities by the Ministry of Education, Culture, Sports, Science and Technology (MEXT), 2008-2012.

References

1. Nolla CM : The development of the permanent teeth. J Dent Child, 27 : 254-266, 1960.
2. Liversidge HM : Permanent tooth formation as a method of estimating age. Front Oral Biol, 13 : 153-157, 2009.
3. Moyer RE. Handbook of orthodontics. Analysis of the dentition and occlusion. 4th ed. Year Book Medical Publishers ; 1988. p.235-238.
4. Jones KL : Smith's recognizable patterns of human malformation, 4th edition 1988 WB Saunders Company, Philadelphia, USA.
5. Broadbent BH : A new technique and its application to orthodontia. Angle Orthod, 1 : 45-66, 1931.
6. Gottlieb EL, Nelson AH, Vogels DS : 1990 JCO study of orthodontic diagnosis and treatment procedures. 1. Results and trends. J Clin Orthod, 25 : 145-156, 1991.
7. Nakayama E, Sugiura K, Ishibashi H, Oobu K, Kobayashi I, Yoshiura K : The clinical and diagnostic imaging findings of osteosarcoma of the jaw. Dentomaxillofac Radiol, 34 : 182-188, 2005.
8. Dos Santos DT, Costa e Silva APA, Vannier MW, Cavalcanti MGP : Validty of multislice computerized tomography for diagnosis of maxillofacial fractures using an independent workstation. Oral Surg Oral Med Oral Pathol Oral Radiol Endod, 98 : 715-720, 2004.
9. Mahasantipiya PM, Savage NW, Monsour PAJ, Wilson RJ : Narrowing of the inferior dental canal in relation to the lower third molars. Dentomaxilofac Radiol, 34 : 154-163, 2005.
10. Flohr TG, Schaller S, Stierstorfer K, Bruder H, Ohnesorge BM, Schoepf UJ : Multi-detector row CT systems and image-reconstruction techniques. Radiology, 235 : 756-773, 2005.
11. Jaffe TA, Nelson RC, Johnson GA, Lee ER, Yoshizumi TT, Lowry CR, Bullard AB, Delong DM, Paulson EK : Optimization of multiplanar reformations from isotropic data sets acquired with 17-detector row helical CT scanner. Radiology, 238 : 292-299, 2006.
12. Erasmus JJ, Gladish GW, Broemeling L, Sabloff BS, Truong MT, Herbst RS, Munden RF : Interobserver and intraobserver variability in measurement of non-small-cell carcinoma lung lesions : implications for assessment of tumor response. J Clin Oncol, 21 : 2574-2582, 2003.
13. Mozzo P, Procacci C, Tacconi A, Martini PT, Andreis IA : A new volumetric CT machine for dental imaging based on the cone-beam technique : preliminary results. Eur Radiol, 8 : 1558-1564, 1998.
14. Mah JK, Danforth RA, Bumann A : Radiation absorbed in maxillofacial imaging with a new dental computed tomography device. Oral Surg Oral Med Oral Pathol Oral Radiol Endod, 96 : 508-513, 2003.
15. Cavalcanti MG, Vannier MW : Three dimensional computed tomography landmark measurement in craniofacial surgical planning : experimental validation in vitro. J Oral Maxillofac Surg, 57 : 690-694, 1999.

RAPID PUBLICATION

AMERICAN JOURNAL OF medical genetics PART A

A New Ehlers–Danlos Syndrome With Craniofacial Characteristics, Multiple Congenital Contractures, Progressive Joint and Skin Laxity, and Multisystem Fragility-Related Manifestations

Tomoki Kosho,[1]* Noriko Miyake,[2] Atsushi Hatamochi,[3] Jun Takahashi,[4] Hiroyuki Kato,[4] Teruyoshi Miyahara,[5] Yasuhiko Igawa,[6] Hiroshi Yasui,[7] Tadao Ishida,[7] Kurahito Ono,[8] Takashi Kosuda,[9] Akihiko Inoue,[10] Mohei Kohyama,[11] Tadashi Hattori,[12] Hirofumi Ohashi,[13] Gen Nishimura,[14] Rie Kawamura,[1] Keiko Wakui,[1] Yoshimitsu Fukushima,[1] and Naomichi Matsumoto[2]

[1]Department of Medical Genetics, Shinshu University School of Medicine, Matsumoto, Japan

[2]Department of Human Genetics, Yokohama City University Graduate School of Medicine, Yokohama, Japan

[3]Department of Dermatology, Dokkyo Medical University, School of Medicine, Mibu, Japan

[4]Department of Orthopedics, Shinshu University School of Medicine, Matsumoto, Japan

[5]Department of Ophthalmology, Shinshu University School of Medicine, Matsumoto, Japan

[6]Department of Urology, Shinshu University School of Medicine, Matsumoto, Japan

[7]First Department of Internal Medicine, Sapporo Medical University, Sapporo, Japan

[8]Department of Orthopedics, Tomioka General Hospital, Tomioka, Japan

[9]Department of Pediatrics, Tomioka General Hospital, Tomioka, Japan

[10]Department of Surgery, Tomioka General Hospital, Tomioka, Japan

[11]Department of Surgery, JA Hiroshima General Hospital, Hiroshima, Japan

[12]Department of Orthopedics, Aichi Children's Health and Medical Center, Oobu, Japan

[13]Division of Medical Genetics, Saitama Children's Medical Center, Saitama, Japan

[14]Department of Radiology, Tokyo Metropolitan Kiyose Children's Hospital, Kiyose, Japan

Received 27 January 2010; Accepted 13 April 2010

We previously described two unrelated patients showing characteristic facial and skeletal features, overlapping with the kyphoscoliosis type Ehlers–Danlos syndrome (EDS) but without lysyl hydroxylase deficiency [Kosho et al. (2005) Am J Med Genet Part A 138A:282–287]. After observations of them over time and encounter with four additional unrelated patients, we have concluded that they represent a new clinically recognizable type of EDS with distinct craniofacial characteristics, multiple congenital contractures, progressive joint and skin laxity, and multisystem fragility-related manifestations. The patients exhibited strikingly similar features according to their age: *craniofacial*, large fontanelle, hypertelorism, short and downslanting palpebral fissures, blue sclerae, short nose with hypoplastic columella, low-set and rotated ears, high palate, long philtrum, thin vermilion of the upper lip, small mouth, and micro-retrognathia in infancy; slender and asymmetric face with protruding jaw from adolescence; *skeletal*, congenital contractures of fingers, wrists, and hips, and talipes equinovarus with anomalous insertions of flexor muscles; progressive joint laxity with recurrent dislocations; slender and/or cylindrical fingers and

Additional supporting information may be found in the online version of this article.

Grant sponsor: Research on Intractable Diseases, Ministry of Health, Welfare, and Labor, Japan; Grant Number: #2141039040; Grant sponsor: Shinshu Association for the Advancement of Medical Sciences; Grant sponsor: Grant-in-Aid for Exploratory Research of Young Scientists, Shinshu University.

*Correspondence to:
Tomoki Kosho, M.D., Department of Medical Genetics, Shinshu University School of Medicine, 3-1-1 Asahi, Matsumoto 390-8621, Japan.
E-mail: ktomoki@shinshu-u.ac.jp

Published online 14 May 2010 in Wiley InterScience
(www.interscience.wiley.com)
DOI 10.1002/ajmg.a.33498

progressive talipes valgus and cavum or planus, with diaphyseal narrowing of phalanges, metacarpals, and metatarsals; pectus deformities; scoliosis or kyphoscoliosis with decreased physiological curvatures of thoracic spines and tall vertebrae; *cutaneous*, progressive hyperextensibility, bruisability, and fragility with atrophic scars; fine palmar creases in childhood to acrogeria -like prominent wrinkles in adulthood, recurrent subcutaneous infections with fistula formation; *cardiovascular*, cardiac valve abnormalities, recurrent large subcutaneous hematomas from childhood; *gastrointestinal*, constipation, diverticula perforation; *respiratory*, (hemo)pneumothorax; and *ophthalmological*, strabismus, glaucoma, refractive errors.

Key words: a new type Ehlers–Danlos syndrome; craniofacial characteristics; multiple congenital contractures; joint laxity; talipes deformities; kyphoscoliosis; skin laxity; multisystem fragility; recurrent subcutaneous hematomas

How to Cite this Article:
Kosho T, Miyake N, Hatamochi A, Takahashi J, Kato H, Miyahara T, Igawa Y, Yasui H, Ishida T, Ono K, Kosuda T, Inoue A, Kohyama M, Hattori T, Ohashi H, Nishimura G, Kawamura R, Wakui K, Fukushima Y, Matsumoto N. 2010. A new Ehlers–Danlos syndrome with craniofacial characteristics, multiple congenital contractures, progressive joint and skin laxity, and multisystem fragility-related manifestations.
Am J Med Genet Part A 152A:1333–1346.

INTRODUCTION

The Ehlers–Danlos syndrome (EDS) is a heterogeneous group of heritable connective tissue disorders affecting as many as 1 in 5,000 individuals, characterized by joint and skin laxity, and tissue fragility [Steinmann et al., 2002]. The fundamental mechanisms of EDS are known to consist of dominant-negative effects or haploinsufficiency of mutant procollagen α-chains and deficiency of collagen-processing-enzymes [Mao and Bristow, 2001]. In a revised nosology, Beighton et al. [1998] classified EDS into six major types: (1) classical type (OMIM#130000) (causative gene, *COL5A1* or *COL5A2*; affected protein, α1(V) or α2(V) procollagen), (2) hypermobility type (OMIM#130020) (*TNXB*; tenascin-XB, in a small subset of cases), (3) vascular type (OMIM#130050) (*COL3A1*; α1(III) procollagen), (4) kyphoscoliosis type (OMIM#225400) (*PLOD*; lysyl hydroxylase), (5) arthrochalasia type (OMIM#130060) (*COL1A1* or *COL1A2*; α1(I) or α2(I) procollagen), and (6) dermatospraxis type (OMIM#225410) (*ADAMTS2*; procollagen I N-proteinase). Additional minor variants of EDS have been identified with molecular and biochemical abnormalities: Brittle cornea syndrome (OMIM#229200) (*ZNF469*) [Abu et al., 2008], EDS-like syndrome due to tenascin-XB deficiency (OMIM#606408) (*TNXB*; tenascin-XB) [Schalkwijk et al., 2001], progeroid form (OMIM#130070) (*β4GALT7*; xylosylprotein 4-beta-galactosyltransferase) [Kresse et al., 1987], cardiac valvular form (OMIM#225320) (*COL1A2*; α2(I) procollagen) [Schwarze et al., 2004], and EDS-like spondylocheirodysplasia (OMIM#612350) (*SLC39A13*; a membrane-bound zinc transporter) [Giunta et al., 2008].

We previously described two unrelated patients showing characteristic facial and skeletal features, with similarities to kyphoscoliosis type EDS but without lysyl hydroxylase deficiency [Kosho et al., 2005]. After observations of them over time and encounter with four additional unrelated patients including one reported by Yasui et al. [2003], we have concluded that they represent a new clinically recognizable type of EDS characterized by distinct craniofacial features, multiple congenital contractures, progressive joint and skin laxity, and progressive multisystem complications associated with tissue fragility including recurrent large subcutaneous hematomas. Here, we present detailed clinical courses of the six patients to delineate the disorder.

CLINICAL REPORTS

Patient 1

The patient is a now 16-year-old Japanese girl. Part of her history was described previously [Kosho et al., 2005]. She was the first child of a healthy mother and a healthy non-consanguineous father, both 19 years of age. She was born by normal vaginal delivery at 42 weeks of gestation. Her birth weight was 2,724 g (−1.3 SD), length 50.0 cm (−0.1 SD), and OFC 32.5 cm (−1.0 SD). She was admitted for the treatment of hypoglycemia, hyperbilirubinemia, and left talipes equinovarus (Fig. 1J). Her craniofacial features included a large fontanelle, hypertelorism, short and downslanting palpebral fissures, blue sclerae, a short nose with a hypoplastic columella, low-set and rotated ears, a high palate, a long philtrum, a thin upper lip vermilion, a small mouth, and micro-retrognathia (Fig. 1A). She had arachnodactyly, flexion-adduction contractures of bilateral thumbs, flexion contractures of the metacarpophalangeal (MP) and interphalangeal (IP) joints in the other fingers (Fig. 1E,F), and rigidity of bilateral hip joints. She suckled poorly, and was admitted again for the treatment of dehydration at age 1 month. Talipes equinovarus was treated with serial plaster casts, and was surgically corrected at age 2 years. Anomalous insertions of the flexor muscles were observed at the operation. Gross motor development was delayed: she sat at age 10 months and walked unassisted at age 2 years. Her skin was easily torn, but showed normal hemostasis in open wounds. Her face became longer with bushy and arched eyebrows and a pointed chin (Fig. 1B). At age 4 years, she developed a large subcutaneous hematoma over the occiput after falling, followed by acute hemorrhagic anemia that required admission and transfusion of hemostatic agents and packed red cells. During the admission, she was suspected to have EDS. At age 6 years, she developed a large subcutaneous hematoma over the temporo-occipital region after falling, requiring admission and intravenous administration of hemostatic agents. She had recurrent dislocations of the shoulders, elbows, and knees.

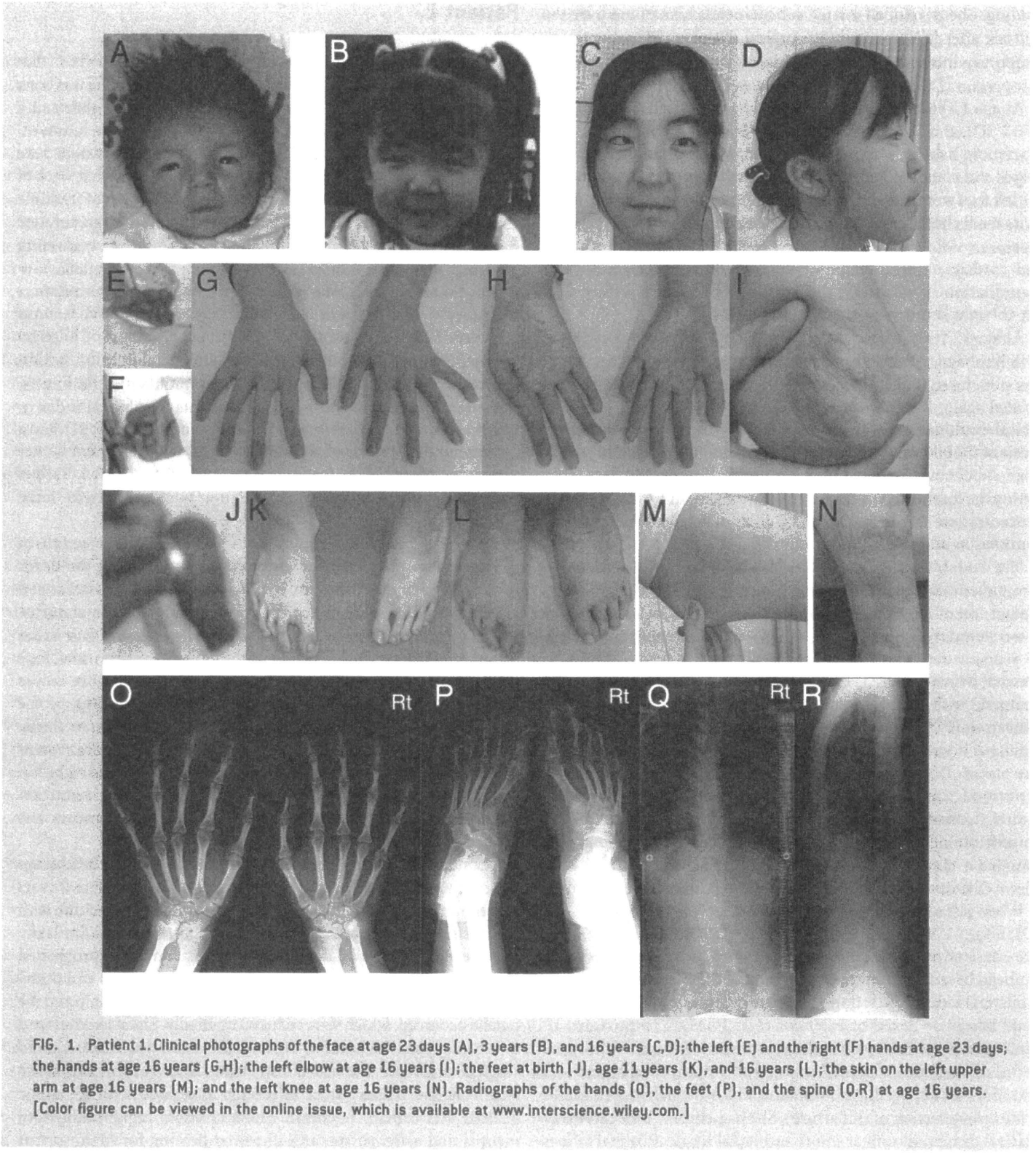

FIG. 1. Patient 1. Clinical photographs of the face at age 23 days (A), 3 years (B), and 16 years (C,D); the left (E) and the right (F) hands at age 23 days; the hands at age 16 years (G,H); the left elbow at age 16 years (I); the feet at birth (J), age 11 years (K), and 16 years (L); the skin on the left upper arm at age 16 years (M); and the left knee at age 16 years (N). Radiographs of the hands (O), the feet (P), and the spine (Q,R) at age 16 years. [Color figure can be viewed in the online issue, which is available at www.interscience.wiley.com.]

When first seen by us at age 7 years, she weighed 19.2 kg (−1.0 SD), height 123.8 cm (+0.8 SD), and OFC 51.5 cm (±0 SD). She had generalized joint laxity, a straight back with scoliosis, and cylindrical and slender fingers. Her skin was hyperextensible, bruisable, and fragile with multiple atrophic scars. Hyperalgesia to pressure such as measuring blood pressure at the upper arms was noted. Ophthalmological examinations showed microcornea and hyperopia. Otological examinations showed narrow middle ear spaces and hearing impairment of high-pitched sounds. Heart murmurs were not audible, and cardiac ultrasonography showed trivial mitral valve regurgitation. Her bladder was dilated with urinary retention and frequent cystitis, requiring manual pressure